BOUNDARY-INTEGRAL EQUATIONS IN EDDY-CURRENT CALCULATIONS

Kim Murphy and Harold A. Sabbagh
Sabbagh Associates, Inc.
4635 Morningside Drive
Bloomington, IN 47408

INTRODUCTION

Volume-integral equations have proven to be very successful in the computation of eddy-current probe-flaw responses for NDE problems having a number of simple geometries. This approach to NDE computations has proven superior to the finite-element approach in both accuracy and computer resources required, and is the basis of our proprietary code VIC-3D[1]. The volume-integral approach, however, is not as well adapted to accommodating the complex geometries sometimes required in practical applications. An example is the separation of edge and corner effects from the response of a flaw. We will discuss an extension of the volume-integral approach that incorporates boundary-integral equations to provide a description of complicated surface geometries.

BACKGROUND

Requirements for eddy-current probe simulation software for the aerospace industry include

1. Coil Modeling:
    1 conventional absolute and differential coils (side mount and end mount),
    2 single eddy-current array probe (ECAP) coils (air core and ferrite backed),
    3 ECAP arrays (air core and ferrite backed), including interactions between coils.
2. Part Geometry Modeling (aircraft engine components):
    1 sharp edges,
    2 chamfered and filleted edges,
    3 bolt holes,
    4 dovetail contours.
3. Defect Modeling:

[1] VIC-3D is a registered trademark of Sabbagh Associates, Inc.

Review of Progress in Quantitative Nondestructive Evaluation, Vol. 14
Edited by D.O. Thompson and D.E. Chimenti, Plenum Press, New York, 1995

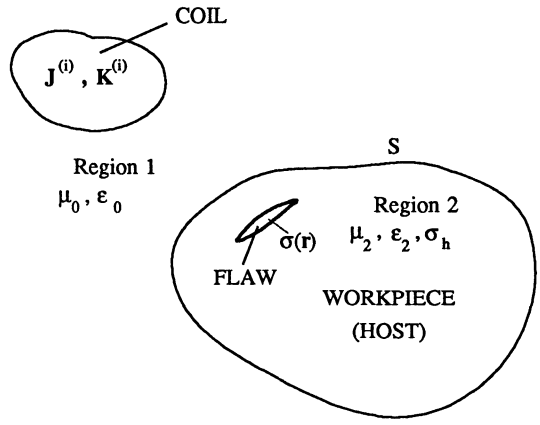

Figure 1: Electromagnetic NDE problem to be solved. Region 1 contains the probe coil, and region 2 the workpiece (or host) and flaw.

1 EDM notches,

2 idealized cracks away from edges,

3 idealized cracks at edges,

4 pits and other geometrically defined defects.

4. Coil Surface Interaction:

1 compute the complex impedance due to coil surface interaction

2 compute lift-off resulting from any combination of coil and geometry models

3 calculate complex impedance as a function of drive frequency.

VIC-3D already solves most of these problems quite efficiently using volume-integral equations [1-3]. We propose to couple boundary-integral equations to the volume-integral equations to enhance VIC's ability to solve the complex geometries of item 2, while, at the same time, distinguishing flaws at edges and corners, as described in item 3.

THE TWO SYSTEMS OF COUPLED INTEGRAL EQUATIONS

We will derive the equations for the general electromagnetic NDE problem, which consists of two regions, as in Figure 1. The first is the exterior of the workpiece, contains the probe coil, and consists of free-space, whereas the second is the finite workpiece which contains a flaw. The boundary of region 2 is labeled S. The ''incident'' fields established by the volume currents produce ''scattered'' fields at boundary S. We want to calculate the scattered fields by using boundary-integral equations.

We use the equivalence principle of Figure 2 to determine various boundary-integral equations. The electric surface current, $\mathbf{J}_e$, and magnetic surface current, $\mathbf{K}_e$, of Figure 2(b) are fictitious sources for the scattered and transmitted fields, $\mathbf{E}_1^{(s,t)}$, $\mathbf{H}_1^{(s,t)}$, and $\mathbf{J}_d$, $\mathbf{K}_d$ serve the same purpose for $\mathbf{E}_2^{(s,t)}$, $\mathbf{H}_2^{(s,t)}$ in Figure 2(c). The ''transmitted'' fields, those with the superscript t, are auxiliary fields, whereas the ''scattered'' fields, those

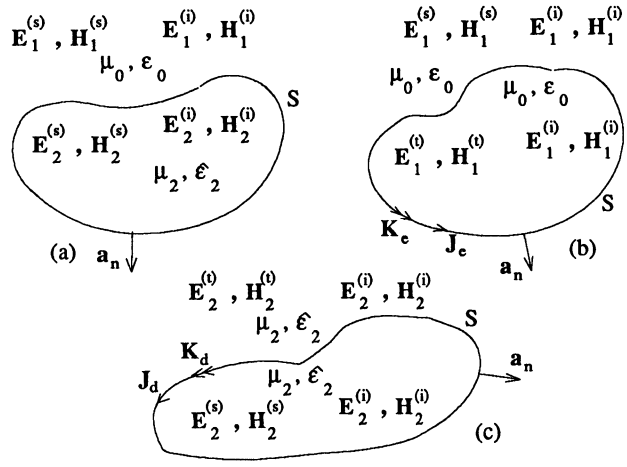

Figure 2: Equivalence principle. (a) Original problem. (b) External equivalence case. (c) Internal equivalence case.

with the superscript s, are actual. We define the surface currents by $\mathbf{J}_s = \mathbf{a}_n \times \mathbf{H}$, and $\mathbf{K}_s = -\mathbf{a}_n \times \mathbf{E}$.

One can derive a host of boundary-integral equations by choosing the auxiliary fields appropriately. For example, if we let $\mathbf{a}_n \times \mathbf{E}_1^{(t)} = 0$, $\mathbf{a}_n \times \mathbf{E}_2^{(t)} = 0$, $\mathbf{a}_n \times \mathbf{H}_1^{(t)} = 0$, $\mathbf{a}_n \times \mathbf{H}_2^{(t)} = 0$, which is Love's equivalence theorem, then it can be easily shown that $\mathbf{J}_e = -\mathbf{J}_d = \mathbf{J}_s$, $\mathbf{K}_e = -\mathbf{K}_d = \mathbf{K}_s$. Using these facts we can derive the following system:

$$j\omega(\hat{\epsilon}_2 + \epsilon_0)\mathbf{K}_s(\mathbf{r}) = 2j\omega\mathbf{a}_n \times (\epsilon_0\mathbf{E}_1^{(i)} - \hat{\epsilon}_2\mathbf{E}_2^{(i)})$$
$$-\mathbf{a}_n \times \frac{1}{2\pi}\int_{S^*}[\mathbf{J}_s(-k_2^2\phi_2 + k_0^2\phi_1) + j\omega\mathbf{K}_s \times \nabla'(\hat{\epsilon}_2\phi_2 - \epsilon_0\phi_1) + \nabla'_s \cdot \mathbf{J}_s\nabla'(\phi_2 - \phi_1)]dS' \quad (1)$$

$$j\omega(\mu_0 + \mu_2)\mathbf{J}_s(\mathbf{r}) = j\omega 2\mathbf{a}_n \times (\mu_2\mathbf{H}_2^{(i)} - \mu_0\mathbf{H}_1^{(i)})$$
$$+\mathbf{a}_n \times \frac{1}{2\pi}\int_{S^*}[\mathbf{K}_s(-k_2^2\phi_2 + k_0^2\phi_1) - j\omega\mathbf{J}_s \times \nabla'(\mu_2\phi_2 - \mu_0\phi_1) + \nabla'_s \cdot \mathbf{K}_s\nabla'(\phi_2 - \phi_1)]dS' \quad (2)$$

$$\mathbf{J}_a(\mathbf{r}) - \sigma_a(\mathbf{r})\int_{\text{flaw}} \mathcal{G}_2^{ee}(\mathbf{r}|\mathbf{r}') \cdot \mathbf{J}_a(\mathbf{r}')dv' =$$
$$-\sigma_a(\mathbf{r})\frac{1}{4\pi}\int_S [j\omega\mu_2\mathbf{J}_s\phi_2(\mathbf{r}|\mathbf{r}') + \mathbf{K}_s \times \nabla'\phi_2(\mathbf{r}|\mathbf{r}') + \frac{1}{j\omega\hat{\epsilon}_2}\nabla'_s \cdot \mathbf{J}_s\nabla'\phi_2(\mathbf{r}|\mathbf{r}')]dS' \ . \quad (3)$$

A second system of boundary-integral equations can be obtained by letting the tangential components of $\mathbf{a}_n \times \mathbf{E}_1^{(t)} = \mathbf{a}_n \times \mathbf{E}_1^{(s)}$, which implies that $\mathbf{K}_e = 0$, as can be seen from Figure 2(b). Similarly, let $\mathbf{a}_n \times \mathbf{E}_2^{(t)} = \mathbf{a}_n \times \mathbf{E}_2^{(s)}$, which means that $\mathbf{K}_d = 0$. Hence, the magnetic surface currents vanish, and we are left with only electric surface currents to be determined. The equations for these currents, $\mathbf{J}_e$, $\mathbf{J}_d$, are obtained by returning to Figure 2(a), and equating the tangential components of the total electric and magnetic fields. The result is

$$\left(\mathbf{E}_2^{(i)} - \mathbf{E}_1^{(i)}\right)_{\tan} = \left\{\frac{1}{4\pi}\int_S \left[j\omega\mu_0\mathbf{J}_e\phi_1(\mathbf{r}|\mathbf{r}') + \frac{1}{j\omega\epsilon_0}\nabla'_s \cdot \mathbf{J}_e\nabla'\phi_1(\mathbf{r}|\mathbf{r}')\right]dS'\right.$$
$$\left. - \frac{1}{4\pi}\int_S \left[j\omega\mu_2\mathbf{J}_d\phi_2(\mathbf{r}|\mathbf{r}') + \frac{1}{j\omega\hat{\epsilon}_2}\nabla'_s \cdot \mathbf{J}_d\nabla'\phi_2(\mathbf{r}|\mathbf{r}')\right]dS'\right\}_{\tan} \quad (4)$$

$$2\mathbf{a}_n \times \left(\mathbf{H}_2^{(i)} - \mathbf{H}_1^{(i)}\right) = \mathbf{J}_e - \frac{1}{2\pi}\int_S \mathbf{a}_n(\mathbf{r}) \times (\mathbf{J}_e \times \nabla'\phi_1(\mathbf{r}|\mathbf{r}'))dS' + \mathbf{J}_d + \frac{1}{2\pi}\int_S \mathbf{a}_n(\mathbf{r}) \times (\mathbf{J}_d \times \nabla'\phi_2(\mathbf{r}|\mathbf{r}'))dS' \quad (5)$$

$$\mathbf{J}_a(\mathbf{r}) - \sigma_a(\mathbf{r})\int_{\text{flaw}} \mathcal{G}_2^{ee}(\mathbf{r}|\mathbf{r}') \cdot \mathbf{J}_a(\mathbf{r}')dv' = -\sigma_a(\mathbf{r})\frac{1}{4\pi}\int_S \left[j\omega\mu_2\mathbf{J}_d\phi_2(\mathbf{r}|\mathbf{r}') + \frac{1}{j\omega\hat{\epsilon}_2}\nabla'_s \cdot \mathbf{J}_d\nabla'\phi_2(\mathbf{r}|\mathbf{r}')\right] dS' \quad (6)$$

where $\mathbf{r} \in S$ in the boundary-integral operators of (1), (2), (4), and (5), $\nabla'_s \cdot$ is the surface divergence, and $\int_{S^*}$ denotes the principal value. The scalar Green's functions are

$$\phi_1(\mathbf{r},\mathbf{r}') = \frac{e^{-jk_0|\mathbf{r}-\mathbf{r}'|}}{|\mathbf{r}-\mathbf{r}'|}, \qquad \phi_2(\mathbf{r},\mathbf{r}') = \frac{e^{-jk_2|\mathbf{r}-\mathbf{r}'|}}{|\mathbf{r}-\mathbf{r}'|}, \quad (7)$$

and $k_0^2 = \omega^2\mu_0\epsilon_0$, $k_2^2 = \omega^2\mu_2\hat{\epsilon}_2$, $\hat{\epsilon}_2 = \epsilon_2 + \sigma_h/j\omega$, and μ_2, $\hat{\epsilon}_2$ are constants. σ_h is the conductivity of the workpiece, which is taken to be homogeneous, and the anomalous conductivity is defined to be $\sigma_a(\mathbf{r}) = \sigma(\mathbf{r}) - \sigma_h$. Note that σ_a vanishes off the flaw.

System (1) and (2) is a modest extension of the system that appears in [4], in that our system contains terms corresponding to the presence of the incident fields in region 2. Poggio and Miller [5] have developed a system for $\mathbf{K}_s$ and $\mathbf{J}_s$, but their system is of the first kind, whereas (1) and (2) are of the second kind. Systems of the second kind usually result in better conditioned matrix equations, which provides significant advantages in numerical computations.

System (4) and (5), like the previous one, has four surface current components as unknowns. It consists of a first-kind integral equation, (4), and a second-kind integral equation, (5). The first equation is the electric-field integral equation (EFIE), and the second the magnetic-field integral equation (HFIE). EFIE's and HFIE's, as individual equations, are well known and understood in the computational electromagnetics community [5]. MacCamy and Stephan [6], and Wang and Ida [7] have used a similar system to solve eddy-current problems.

In both of these systems, $\mathbf{J}_a(\mathbf{r})$ is the anomalous current density that is associated with the flaw. Equations (3) and (6) are volume-integral equations for the anomalous current. These same equations (with a different right-hand side, of course) are already solved very efficiently in VIC-3D.

The incident fields in region 1 are due to the exciting coil. Hence, we have

$$\mathbf{E}_1^{(i)}(\mathbf{r}) = \int_{\text{coil}} \mathcal{G}_1^{ee}(\mathbf{r}|\mathbf{r}') \cdot \mathbf{J}_c(\mathbf{r}')dv' \quad (8)$$

$$\mathbf{H}_1^{(i)}(\mathbf{r}) = \int_{\text{coil}} \mathcal{G}_1^{me}(\mathbf{r}|\mathbf{r}') \cdot \mathbf{J}_c(\mathbf{r}')dv', \quad (9)$$

whereas those in region 2 are given by integrals over the region of the flaw:

$$\mathbf{E}_2^{(i)}(\mathbf{r}) = \int_{\text{flaw}} \mathcal{G}_2^{ee}(\mathbf{r}|\mathbf{r}') \cdot \mathbf{J}_a(\mathbf{r}')dv' \quad (10)$$

$$\mathbf{H}_2^{(i)}(\mathbf{r}) = \int_{\text{flaw}} \mathcal{G}_2^{me}(\mathbf{r}|\mathbf{r}') \cdot \mathbf{J}_a(\mathbf{r}')dv'. \quad (11)$$

$\mathcal{G}$ is a dyadic Green's function whose subscript defines its region, and whose superscripts denote its type. The first superscript denotes the nature

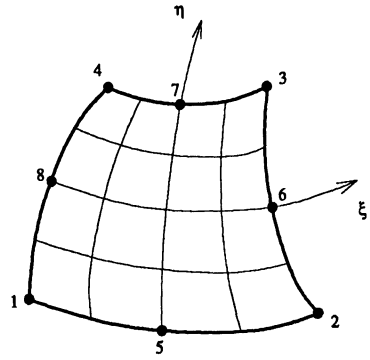

Figure 3: Eight-node serendipity element.

of the field at r, e being electric, and m magnetic, whereas the second superscript denotes the nature of the source at r'. $\mathcal{G}_1$ is determined from ϕ_1, and $\mathcal{G}_2$ from ϕ_2.

The integral equations are discretized by means of Galerkin's variant of the method of moments. The anomalous current, $\mathbf{J}_a(\mathbf{r})$, is expanded in three-dimensional pulse functions that are defined on a regular grid, and the resulting equation is then tested with the same functions. This results in a matrix equation in which the matrix is Toeplitz in all three dimensions:

$$\mathbf{G}(jlm, JLM) = \mathbf{G}^{(0)}(l - L, m - M, j - J) \ . \tag{12}$$

This feature gives VIC-3D its ability to solve very large problems efficiently on personal computers with a minimum of storage. (We have solved problems with 50,000 unknowns in a day, using less than 20MB on a personal computer.)

DISCRETIZATION OF THE BOUNDARY-INTEGRAL OPERATORS

The discretization of the boundary-integral operators also uses Galerkin's variant of the method of moments, except that the unknown surface currents are expanded in vector edge-elements that are defined on a surface mesh [13-14]. These elements preserve continuity of normal components of the currents across edges of the mesh, thereby guaranteeing that the unknown currents belong to $H(div)$, the space of square-integrable functions, whose divergences are also square-integrable.

We have developed a theory of higher-order edge-elements (i.e., elements that interpolate to higher-order than linear), which is implemented using the eight-node serendipity element of finite-element theory [8]. The element is shown in Figure 3, and the interpolating polynomials are listed in (13).

$$\begin{aligned}
&\text{Eight-node serendipity quadrilateral :} \\
&\psi_1(\xi,\eta) = [(1-\xi)(1-\eta) - (1-\xi^2)(1-\eta) - (1-\eta^2)(1-\xi)]/4 \\
&\psi_2(\xi,\eta) = [(1+\xi)(1-\eta) - (1-\xi^2)(1-\eta) - (1-\eta^2)(1+\xi)]/4 \\
&\psi_3(\xi,\eta) = [(1+\xi)(1+\eta) - (1-\xi^2)(1+\eta) - (1-\eta^2)(1+\xi)]/4 \\
&\psi_4(\xi,\eta) = [(1-\xi)(1+\eta) - (1-\xi^2)(1+\eta) - (1-\eta^2)(1-\xi)]/4 \\
&\psi_5(\xi,\eta) = (1-\xi^2)(1-\eta)/2 \\
&\psi_6(\xi,\eta) = (1-\eta^2)(1+\xi)/2 \\
&\psi_7(\xi,\eta) = (1-\xi^2)(1+\eta)/2 \\
&\psi_8(\xi,\eta) = (1-\eta^2)(1-\xi)/2.
\end{aligned} \tag{13}$$

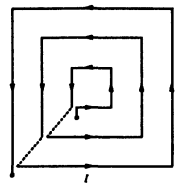

Figure 4: A printed-circuit coil.

One can expand both the geometry of the workpiece and the surface currents using (13) for interpolation, which makes this an isoparametric element. If, however, the order of the geometric shape function is greater than the order of approximation of the fields, then the geometric elements are called *superparametric*; conversely, the geometric elements are called *subparametric* if their order is less than that of the field shape elements [9]. There are advantages to using different orders of approximation of the geometry and fields. Ingber and Ott [9] have gotten good results when approximating the geometry to second order, while approximating the currents with linear shape functions. This means that there may be fewer variables required to represent the field than to represent the geometry, with a consequent reduction in computer resources to solve for the fields.

The interpolating vector-basis functions are given by

$$\begin{aligned} \mathbf{f}_{i1} &= \psi_i(\xi,\eta)\frac{\mathbf{a}_\xi}{\mathbf{a}_n\cdot(\mathbf{a}_\xi\times\mathbf{a}_\eta)} = \psi_i(\xi,\eta)\frac{\mathbf{a}_\xi}{\boldsymbol{\tau}_\xi\cdot\mathbf{a}_\xi} \\ \mathbf{f}_{i2} &= \psi_i(\xi,\eta)\frac{\mathbf{a}_\eta}{\mathbf{a}_n\cdot(\mathbf{a}_\xi\times\mathbf{a}_\eta)} = \psi_i(\xi,\eta)\frac{\mathbf{a}_\eta}{\boldsymbol{\tau}_\eta\cdot\mathbf{a}_\eta} \end{aligned} \quad . \tag{14}$$

The vectors $\mathbf{a}_\xi$ and $\mathbf{a}_\eta$ are the unit tangent vectors to the surface along the ξ and η directions, while $\mathbf{a}_n$ is the unit normal to the surface. The vector, $\boldsymbol{\tau}_\xi$, is normal to the ξ = constant curve, and points in the direction of increasing ξ. Thus, $\boldsymbol{\tau}_\xi$ is normal to $\mathbf{a}_\eta$. $\boldsymbol{\tau}_\eta$ is normal to the η = constant curve, and points in the direction of increasing η. Thus, $\boldsymbol{\tau}_\eta$ is normal to $\mathbf{a}_\xi$. The interpolating vector-basis functions satisfy $\boldsymbol{\tau}_\xi\cdot\mathbf{f}_{i1}=1$, at the ith node, and vanish at the other nodes; $\boldsymbol{\tau}_\eta\cdot\mathbf{f}_{i2}=1$ at the ith node, and vanishes at the other nodes.

We have developed a method of handling the improper integrals that occur in computing the matrix elements of the boundary-integral operators. This algorithm, which is based on an idea of Hayami [10], requires one to locate the field point that is nearest the source region, and then translating the origin of coordinates to this point. The computation is then completed in a polar coordinate system, which has the effect of removing the singularity.

ANALYSIS OF PRINTED-CIRCUIT AND SPLIT-CORE DIFFERENTIAL PROBES

The model will include the incident fields of (8) and (9) that are produced by the printed-circuit coil of Figure 4 and the split-core differential probe of Figure 5.

Arrays of printed-circuit coils are becoming prominent in precision

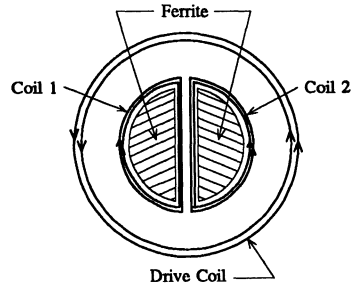

Figure 5: A split-core differential probe.

measurements of complex shapes, such as dovetail slots in aircraft turbine disks [11]. A significant advantage of such arrays is that they are fixed in space on the part, and no mechanical scanning is required. We apply the electromagnetic reaction principle [12] to develop expressions for the driving-point and transfer-impedances of such arrays. The essential step is the calculation of the reaction between the field produced by the coil and the anomalous current within the flaw:

$$[i,a] = \int\int\int_{flaw} \mathbf{E}^{(i)} \cdot \mathbf{J}^{(a)} dV \ . \tag{15}$$

In (15) $\mathbf{E}^{(i)}$ is the incident electric field within the flaw, produced by one ampere in the printed-circuit coil, and $\mathbf{J}^{(a)}$ is the anomalous current within the flaw.

The split-core differential probe is also used in studying complex shapes. It consists of two identical ferrite cores, around each of which is a coil. The arrangement produces a differential signal, which is the difference of the signals seen by each of the two parts when the probe is scanned over a flaw. The differential probe is sensitive to edges, and not to slowly varying background conditions.

REFERENCES

1. Sabbagh Associates, Inc. ''An Eddy-Current Model For Three-Dimensional Nondestructive Evaluation of Advanced Composites,'' Final Report, Naval Surface Warfare Center - White Oak, Silver Spring, MD, 25 July, 1988.
2. L. D. Sabbagh, H. A. Sabbagh, ''A Computer Model of Eddy-Current Probe-Crack Interaction,'' Review of Progress in Quantitative Nondestructive Evaluation, Brunswick, ME, July, 1989
3. L. D. Sabbagh, K. H. Hedengren, D. C. Hurley, ''Interaction of Flaws with a Ferrite-Core Eddy Current Probe: Comparison between Model and Experiment,'' D. O. Thompson and D. E. Chimenti, editors, *Review of Progress in Quantitative Nondestructive Evaluation Vol 10A*, p 883, Plenum, New York, 1991.
4. C. Müller, *Foundations of the Mathematical Theory of Electromagnetic Waves*. New York: Springer-Verlag, 1969.
5. A. J. Poggio and E. K. Miller, ''Integral Equation Solutions of Three-dimensional Scattering Problems'', in R. Mittra, ed., *Computer Techniques for Electromagnetics*, Chapter 4. Oxford: Pergamon Press, 1973.

6. R. C. MacCamy and E. Stephan, ''Solution Procedures for Three-Dimensional Eddy Current Problems,'' J. Mathematical Analysis and Applications, Vol. 101, pp. 348-379, 1984.
7. J-S. Wang and N. Ida, ''Utilization of Geometric Symmetries in ''Edge'' Based Boundary Integral Eddy Current Solutions,'' IEEE Trans. Magnetics, Vol. 28, No. 2, March 1992, pp. 1704-1707.
8. T. J. R. Hughes, *The Finite Element Method: Linear Static and Dynamic Finite Element Analysis*. Englewood Cliffs: Prentice-Hall, 1987.
9. M. S. Ingber and R. H. Ott, ''An Application of the Boundary Element Method to the Magnetic Field Integral Equation,'' IEEE Trans. Antennas and Propagation, Vol. 39, No. 5, May 1991, pp. 606-611.
10. K. Hayami, ''High Precision Numerical Integration Methods for 3-D Boundary Element Analysis,'' IEEE Trans. Magnetics, Vol. 26, No. 2, March 1990, pp. 603-606.
11. D. C. Hurley, K. H. Hedengren, and J. D. Young, in *Review of Progress in QNDE*, vol. 11, eds. D. O. Thompson and D. E. Chimenti (Plenum, New YOrk, 1992), p. 1137.
12. R. F. Harrington, *Time-Harmonic Electromagnetic Fields*. New York: McGraw-Hill, 1961.
13. Z. J. Cendes, ''Vector Finite Elements for Electromagnetic Field Computation,'' IEEE Trans. Magnetics, Vol. 27, No. 5, September 1991, pp. 3958-3966.
14. A. Bossavit and I. Mayergoyz, ''Edge-Elements for Scattering Problems,'' IEEE Trans. Magnetics, Vol. 25, No. 4, July 1989, pp. 2816-2821.